Pixel Sensitivity Correction of Varex Amorphous Silicon EPID for High Dose Rate Brachytherapy

Yuen, M.Y.Y.

Abstract

The aim of this study is to determine the pixel sensitivity of the amorphous silicon electronic portal imaging device (EPID) and to finally develop a correction method for imaging with a HDR brachy source. As a result, these images can be improved. For the calibration method, the MV-source of a linear accelerator (linac) and the kV-source of a cone beam CT (CBCT) have been used to irradiate the EPID with the same field while the panel is shifted between each irradiation. One dataset using the linac and two datasets using the CBCT have been acquired which resulted in three different pixel sensitivity maps (PSM). The PSMs have been applied on an evaluation image acquired with a HDR Ir-192 source. The calibration method of the third PSM has performed the best since the noise level in the corrected evaluation image has reduced the most with 52.5 to 54.8% compared to the RAW image. It can be concluded that this correction method gives positive results, however, the synchronization problem of the EPID with the linac or CBCT should be looked further into.

Keywords— EPID dosimetry, HDR Brachytherapy, Response corrections, Pixel sensitivity map, Calibration

1 Introduction

Brachytherapy (BT) is a radiotherapy modality that places radioactive sources within or very close to the cancerous tissue [1, 2]. This treatment modality is broadly used to treat a wide variety of cancers of which currently prostate and gynecologic sites are the most common to administer BT [2–4]. BT can also be used to treat other malignancies such as, skin, breast, head and ocular. Compared to external beam radiotherapy (EBRT), BT makes use of radioactive source. These sources can be implanted permanently into the body or temporarily using remote afterloading where the radioactive sources comes from a sealed safe, going through catheters and positioning them close to or into the target tissue, and are subsequently retracted back into the sealed safe after the radiation is deposited to the target tissue. BT has the advantage that it is characterized by a steep dose fall-off. This indicates that a high dose of radiation can be delivered to the target within millimeters of the source while the adjacent healthy tissue outside this range will receive a much lower dose compared to the target. This will result in a successful treatment outcome with less toxicity [1, 3, 4]. For HDR BT, high doses of radiation are delivered to the target in a short period of time, small positioning uncertainties of the radiation source can result in a poorly treated tumor and unnecessary damage to healthy tissue [4]. For this reason, it is crucial that the dose is delivered very accurately to the target. Currently, treatment verification in real time is not used as a golden standard in hospitals because of the lack of proper BT treatment monitoring devices [5]. As a consequence, treatment errors frequently go unnoticed which can affect many patients [6]. Therefore, there is a critical need for treatment verification systems in real time since it can improve patient safety and treatment outcome.

The use of an amorphous silicon electronic portal imaging device (a-Si EPID) as treatment verification tool for HDR BT, is of current interest since EPIDs are already commonly employed in the clinic for EBRT [4]. The EPID can measure the gamma ray intensity which has travelled through the patient from a radiation source during treatment [7]. This way, the gamma rays are converted in the caesium-iodine (CsI) scintillator of the a-Si EPID into visible light which is detected by the single substrate a-Si active thin-film transistor-photodiode array [8]. Each photodiode is equal to a pixel in an image. Hence, a 2D image is produced from this radiation signal [9]. EPIDs were originally developed for the verification of patient positioning [10]. However, it can also be used for dosimetric application. For dosimetry, the EPID pixel sensitivity is of importance since every pixel has a different response to a given irradiation. This is due to the intrinsic electronic variability between components in the EPID panel. Therefore, it is of utmost importance to perform an EPID pixel sensitivity calibration to guarantee a homoge-

neous response of the panel and to reduce artefacts in an image. Frequently, the flood field calibration is performed for imaging applications which irradiates the EPID panel with a large field covering the whole detector. However, this method has limitations for dosimetric applications since the irradiation field is not homogeneous which results in different doses deposited on the panel. This method has the disadvantage that each pixel has a different response to a given irradiation [9].

This study is part of a larger project called Dose and motion measurements in BT (DETERMINE) [11]. It presents a novel dosimetric system called Iradium Imaging System (IrIS) which consists of an EPID and a 3D camera. The EPID is capable of tracking the radiation source inside the patient and the 3D camera is able to monitor the patients' position with respect to the EPID. The aim of the system is to detect possible deviations in real time from the treatment such that treatment errors will be prevented and the truly delivered dose to the patient will become known.

In this research, the focus lies on the evaluation of the Varex Imaging's XRD 4343N EPID panel [12]. It has been mentioned before that the pixel sensitivity calibration is of utmost importance when using an EPID for dosimetry. Therefore, the aim of this work is to correct for the pixel sensitivity of the EPID and to finally use it for imaging with a HDR brachy source so that the correction can improve the image. Firstly, from the calibration method, a pixel sensitivity map (PSM) has to be obtained. This implies that all pixels have the same pixel response (uniform intensity and same energy spectrum) to a given irradiation [13]. To derive the PSM, a linear accelerator (linac) and a cone beam CT (CBCT) have been used to irradiate the EPID with the same field while the panel is shifted between each irradiation. By maintaining the same small irradiation field, the field can be considered homogeneous. During the execution of the experiments, it has been noticed that the EPID was not synchronized with the linac nor CBCT. This means that the EPID is being read out while it is receiving a radiation pulse from the linac or CBCT. The lack of synchronization causes horizontal lines, which are visible in the acquired frames and will effect the PSM. For this reason, different PSMs have been obtained to tackle this problem. The first PSM is acquired using the MV-source of the linac while not taking into account the synchronization problem. In addition, two other PSMs have been acquired while both uses the kV-source of the CBCT. However, the two PSMs contain a different solution to tackle the synchronization problem. Lastly, for the evaluation, images are acquired with a HDR brachy source. The different PSMs are subsequently applied to these images to eventually determine the improvement in dosimetric accuracy. Lastly, the EPID intensity profiles corrected for pixel sensitivity are compared with the original acquired images with HDR brachy source.

2 Methodology

2.1 The EPID panel

The Varex Imaging's XRD 4343N is an amorphous silicon flat panel x-ray detector which is used for high dose applications. The panel supports a full field of view (FOV) of 432x432 mm^2 with a pixel matrix of 2880x2880 pixels and pixel pitch of 150 μm. The pixels are behind a CsI scintillator sheet. The electronics are protected by shielding and it can use energies up to 450 kV. In addition, there are seven FOV options, five gain modes and four binning modes with frame rates up to 115 fps [12]. Further information about the EPID can be found in literature [8].

Furthermore, there are several settings available on the EPID. The gain is the amplification of the signal which defines the sensitivity of the panel. If the input signal is low, the gain should be increased since this increases the sensitivity of the panel. However, setting the gain too high will result in saturation and information will be lost, which has to be avoided. For the different calibration datasets, the gain mode has been adjusted to maintain an adequate signal and to avoid saturation. In addition, binning combines neighbouring pixels which results in faster readout speeds and improves the signal to noise ratio at the price of reduced spatial resolution. For all datasets, a default binning mode of 1x1 has been used since this paper looks into the sensitivity of each pixel. Lastly, the frame rate defines how many frames are acquired per second. Since the images are captured with a continuous acquisition mode and the EPID readout is not synced with the beam pulses, this has been set to a default value of 15 fps. The settings of the three datasets can be found in Table 1.

Table 1: Detector settings of the three datasets

	D1	**D2**	**D3**
Gain mode	1	4	2
Binning	1x1	1x1	1x1
Frame rate (fps)	15	15	15

2.2 Calibration

For the calibration, the EPID is irradiated using a linac with a MV-source and a CBCT with a kV-source. Usually, the linac is used to calibrate the EPID. However, the linac can damage the electronics of this EPID since this EPID can only use energies up to 450 kV. For this reason, both sources are used for

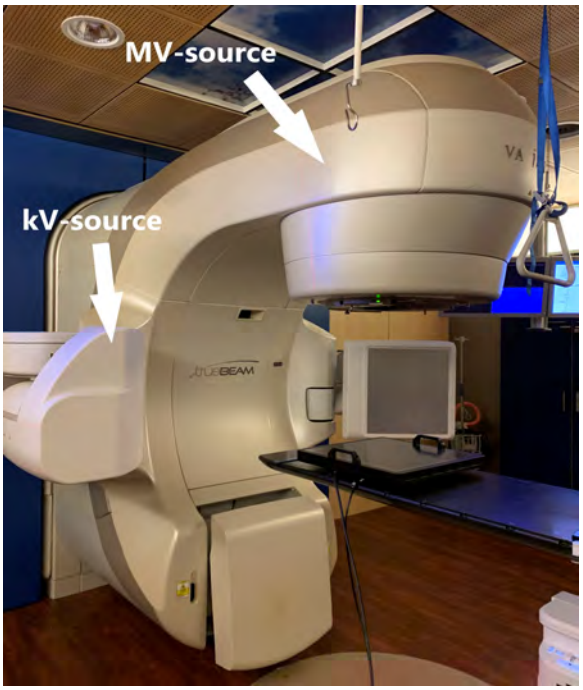

(a) Set-up of the EPID and linac using a MV-source

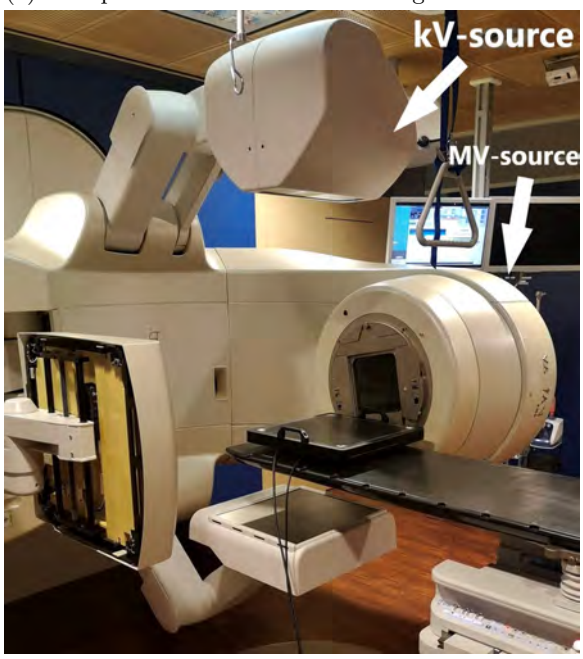

(b) Set-up of the EPID and linac using a kV-source

Figure 1: Set-up of linac and EPID

the calibration and are eventually compared to determine which calibration method performs well. Also, it is expected that the kV-source will perform better since the energy spectrum used for HDR brachytherapy is similar.

Furthermore, the set-up for the calibration of the EPID using a linac and CBCT are shown in Figure 1. The gantry can be rotated which gives the possibility to irradiate the EPID with a MV or kV-source. First, the EPID is placed on the treatment table. Using the linac, the MV-source is placed right above the EPID panel (Figure 1a). For the use of the CBCT, the gantry is rotated 90 degrees in order that the kV-source is located straight above the EPID (Figure 1b).

2.2.1 Acquisition datasets

A total of three datasets have been acquired. To acquire the images, the EPID is irradiated with a linac for the first dataset (D1) and with a CBCT for the second and third dataset (D2, D3) using the same irradiation field while the panel has been displaced with a small shift laterally or longitudinally between each irradiation. This results in one image per field position. Each image is the average of the total number of frames acquired. This information is visualized in Table 2 for a certain field position. The most important detail from this table is that the images of D1 have been acquired by irradiating the EPID using an energy of 6 MV and that the images of D2 and D3 are using an energy of 100 kV.

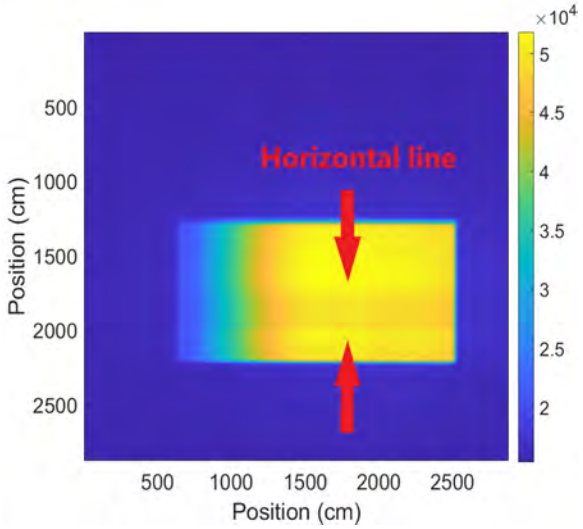

Figure 2: Horizontal line is visible in one of the frames

To tackle the synchronization problem of the EPID with the linac or CBCT, the images of D2 and D3 have been differently acquired (Figure 2). The frames of D2 have been acquired 20 seconds after the beginning of the irradiation to prevent ghosting. Additionally, for the acquisition of the images, the EPID averaged response has been taken over 1000 frames instead of 100 frames. This way, the horizontal lines are averaged out and will not be visible in the PSM. For the images of D3, the image is not averaged over all frames, but are averaged over a subset of frames. This method looks at each pixel in a specific pixel location for all frames and calculates the median value. If the pixel intensity value is smaller than the median value of all frames at that specific pixel location, this frame containing the value will not be taken into ac-

count when calculating the average intensity value for that location. This has been done for all pixel locations. In this manner, the pixel intensity values from the horizontal lines will not be taken into account when calculating the average image over all frames. Lastly, the same response corrections are performed on the three datasets.

Table 2: Information of the acquired PSM datasets. The maximum energy is the maximum energy used of the linac source. The field size is the size of the irradiation field in cm^2. The shift is the displacement in cm between each irradiation. The number of frames is the total number of frames acquired at one position of the EPID. Total field positions is the total number of images (averaged over total number of frames) acquired with the same field at different positions of the panel.

	D1	**D2**	**D3**
Maximum energy (kVp)	6000	100	100
Field size (cm^2)	20x20	24x20	24x12
Shift (cm)	5	3.5	2 - 5
Number of frames	100	1000	100-120
Total field positions	25	48	35

2.2.2 EPID response corrections

Each dataset contains images acquired with the same field at different positions of the EPID. D1, D2 and D3 contain 25, 48 and 35 images in total, respectively (Table 2). The response corrections have been performed on all images of each dataset and are described in this section.

2.2.2.1 Dark field correction

To remove the offset signals of individual pixels in the RAW image and to correct for electronic noise, the dark field (DF) image is acquired. This is an image without the presence of radiation. The DF corrected image is obtained by subtracting the DF image from the acquisitions. In addition, the EPID averaged offset response has been taken over 100 frames without radiation.

2.2.2.2 Dead line correction

The EPID contains a dead pixel line (DL) with intensity values close to zero after subtraction of the DF image. The artefact line, containing the defective pixel intensity values, has been removed by locating these pixel coordinates. Subsequently, the invalid pixel intensity values have been replaced by applying interpolation which uses the intensity values of their neighbors.

2.2.2.3 Pixel sensitivity map

The EPID response of the pixels should be the same during each irradiation if they are located in the same EPID position. The sensitivity for each pixel can be obtained by comparing its individual response against a reference value. Image registration has been used on all images of each dataset to acquire the reference response. For the registration, rigid translation has been applied on the images since the panel is only displaced laterally or longitudinally. Moreover, the imaging modality is specified as monomodal since the images are similar in brightness and contrast. A perfect registration is also necessary since the reference response for each pixel should be accurate. For this reason, prior to the image registration, an initial translation has been applied on the images located at the boundaries to move them in the right direction. After the images are registered, the mean of all pixel values at each pixel location has been taken over these images which gives the reference response. Subsequently, the pixel sensitivity of each pixel can be obtained by dividing each individual pixel response by its reference response. Lastly, by combining the pixel sensitivities for each pixel, the PSM for each dataset can be determined.

The DF and DL corrected image can now be corrected for pixel sensitivity using the following equation:

$$I'(x,y) = \frac{I(x,y)}{PSM(x,y)} \tag{1}$$

2.3 Evaluation

For the evaluation, images are acquired by irradiating a realistic 3D-printed pelvic phantom placed on top of the EPID with an Ir-192 radioactive seed. The phantom contains a transrectal ultrasound probe and three catheters which are connected to the remote afterloader (Figure 3). Additionally, the images are acquired using different detector settings (gain and frame rate).

Figure 3: Set-up using a 3D printed pelvic phantom on top of the EPID containing three inserted needles and a transrectal ultrasound probe

To evaluate the performance of the different obtained PSMs acquired with different energy sources, they are applied on the independent images acquired with a HDR Ir-192 source. First, an intensity map (IM) has been obtained which represents the difference between the RAW image and the corrected image. Subsequently, an intensity profile (single horizontal line) has been taken at panel positions 21.6 and 10.8 cm on the y-axis for the RAW image and the corrected image to observe the difference in EPID response. This profile returns a set of intensity values of all pixels along this line. Lastly, by taking the sum of the absolute value of the difference in intensity value between two consecutive pixel values along the line, the noise level of the image at these positions can be determined:

$$N = \sum_{i=5}^{n-5} |I(x+i-1, y) - I(x+i, y)| \qquad (2)$$

with N the noise level. The intensities at the boundaries have been excluded for the calculation of the noise level since the values are not relevant.

By expressing the difference in noise level between the RAW and corrected image in percentage, the improvement of the noise level can be obtained:

$$N_{imp} = \frac{N_{raw} - N_{corr}}{N_{raw}} * 100\% \qquad (3)$$

3 Results

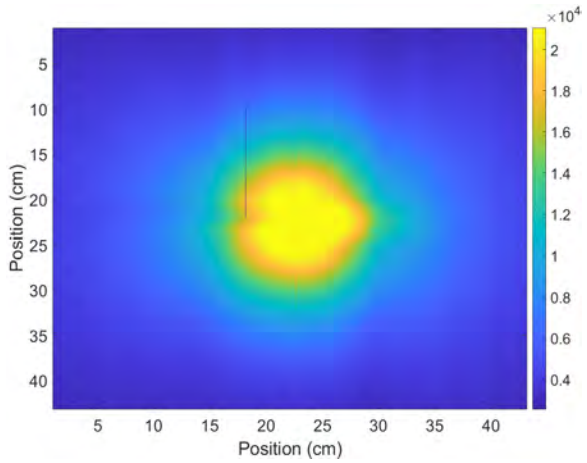

Figure 4: RAW image

Looking at the RAW image in Figure 4, it can be observed that the yellow shape in the center represents the pelvic phantom which is irradiated with a HDR Ir-192 source. The phantom is located in the center between positions 15 and 30 cm on both axis. It can be noticed that there is an artefact occurring at position 18 cm on the x-axis and that the background contain some vertical lines.

Comparing the RAW image with the corrected images (Figures 6a, 6f and 6k), it can be seen that the dead line at position 18 cm on the x-axis does not appear in the corrected images. Looking at the IMs (Figures 6b, 6g and 6l), it can be noticed that the vertical lines are removed from the RAW image. For the IMs of D2 and D3, some high intensity pixels located in the center are removed, in particularly for the IM of D2.

The PSM of each dataset has been acquired and are visualized in Figure 5. Each pixel has an intensity variation in the range of 0.9 and 1.1. It can be noticed that the PSM of D1 (PSM1) contains many horizontal lines covering most of the panel (Figure 5a). For the PSMs of D2 and D3 (PSM2 and PSM3), the horizontal lines are also present (Figures 5b and 5c). However, these horizontal lines only appear at several positions on the panel and contain similar intensity values. Lastly, the boundaries of PSM1 and PSM3 contain some dark blue lines which are pixels with no intensity value.

The EPID response corrections acquired with different datasets have been applied on the images acquired with the HDR Ir-192 source. The intensity profiles for an image of the evaluation dataset is visualized in Figure 6. The intensity profiles are acquired at panel positions 21.6 cm and 10.8 cm on the y-axis showing the data without correction (RAW) and with the correction of the DF, DL and PSM (Corrected). Comparing the RAW and corrected intensity profile of each dataset, the profile is lower in intensity value and the negative spike at position 18 cm on the x-axis has been removed from the profile after correction. Looking at the intensity profiles of PSM1, it can be observed that the noise is not reduced after the response corrections (Figures 6c and 6d). However, having a closer look at the intensity profile at the boundary region, the noise is reduced since the curve is smoother after correction (Figure 6e). In Figure 6h, the intensity profile of PSM2 is shown. It can be seen that the overall intensity profile after correction improves since the noise reduces in all regions (Figures 6i and 6j). This result also holds for the intensity profiles of PSM3 (Figures 6m, 6n and 6o).

The noise level improvements in percentage of each dataset based on the intensity profiles of the RAW image (no correction) and corrected image (corrected with DF, DL and PSM) at positions 21.6 cm and 10.8 cm on the y-axis, have been determined. The value of N_{imp} after correction for all datasets is positive which means that the noise is reduced after the response corrections. The noise in the image is reduced with 22.9% at position 21.6 cm and 24.1% at position 10.8 cm after the response corrections using PSM1. For the response corrections of PSM2 and PSM3, the noise in the image is reduced with 51.8% and 52.5% at position 21.6 cm and 54.7% and 54.8% at position 10.8 cm, respectively. The value of N_{imp} is the high-

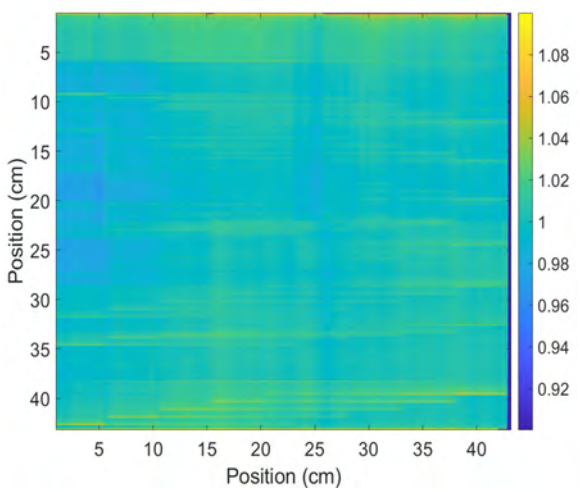

(a) PSM1: PSM acquired with the images of D1

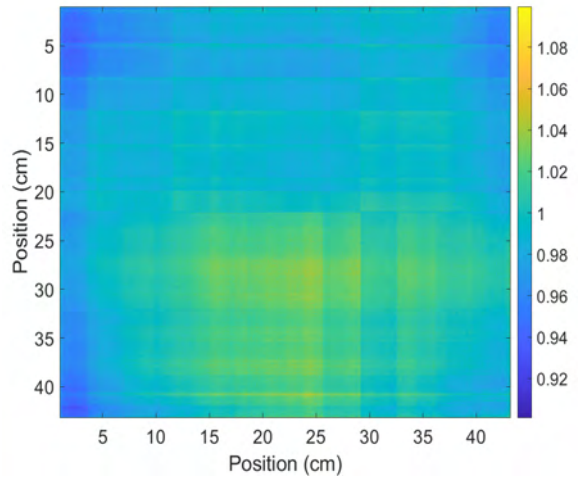

(b) PSM2: PSM acquired with the images of D2

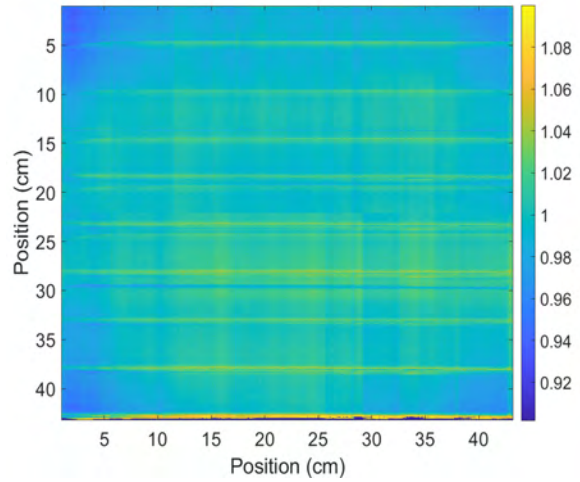

(c) PSM3: PSM acquired with the images of D3

Figure 5: PSMs of the three datasets

est for the correction of PSM3. In addition, to evaluate the noise level improvement based on only the PSM, the RAW image has been corrected for DF and DL and is subsequently compared with the corrected image. The noise level improvements are in Table 4 and it can be observed that the noise level does not improve after the PSM1 correction since the value of N_{imp} is negative. However, this value is positive when applying the corrections of PSM2 and PSM3.

Table 3: Noise level improvements in percentage of each dataset based on the intensity profiles of the RAW image (no correction) and Corrected image (corrected with DF, DL and PSM) at positions 21.6 and 10.8 cm.

	Corrected 21.6 cm	**Corrected 10.8 cm**
N_{imp} of PSM1 [%]	22.9	24.1
N_{imp} of PSM2 [%]	51.8	54.7
N_{imp} of PSM3 [%]	52.5	54.8

Table 4: Noise level improvements in percentage of each dataset based on the intensity profiles of the RAW image (corrected with DF and DL) and Corrected image (corrected with DF, DL and PSM) at positions 21.6 and 10.8 cm.

	Corrected 21.6 cm	**Corrected 10.8 cm**
N_{imp} of PSM1 [%]	-4.9	-6.5
N_{imp} of PSM2 [%]	34.4	36.3
N_{imp} of PSM3 [%]	35.3	36.6

4 Discussion

To use the EPID for dosimetry, the pixel sensitivity calibration is crucial. The aim of this work is to correct for the pixel sensitivity of the EPID and to use it for imaging with a HDR brachy source so that the image improves after the correction.

For the evaluation, all images acquired with the HDR brachy source and different settings have been evaluated. However, only one image has been presented in section 3 since similar results have been observed for all images.

The evaluation image is first corrected for DF and DL. After the DF correction, the intensities become lower in value which can be observed in the intensity profile plots (Figures 6c, 6h and 6m). Also, the vertical lines which appear in the background of the RAW image are removed in the corrected images since these vertical lines are present in the IMs (Figure 4, 6b, 6g and 6l). By removing these vertical lines, the sudden steps in intensity are removed from the intensity profiles which makes the line more smooth, especially at the boundaries (Figures 6e, 6j and 6o). In addition, the artefact line containing the defective pixels have a different response and can be observed around

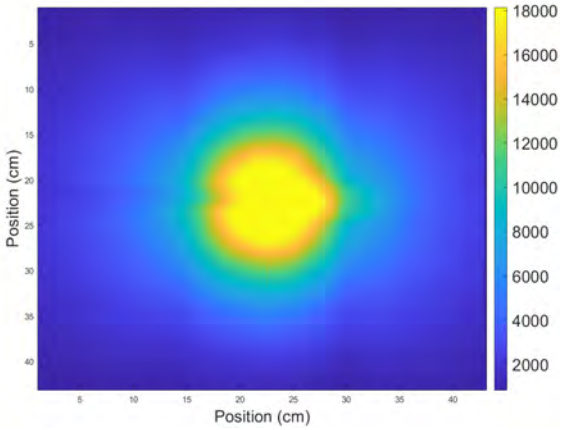

(a) Image after response corrections acquired with D1

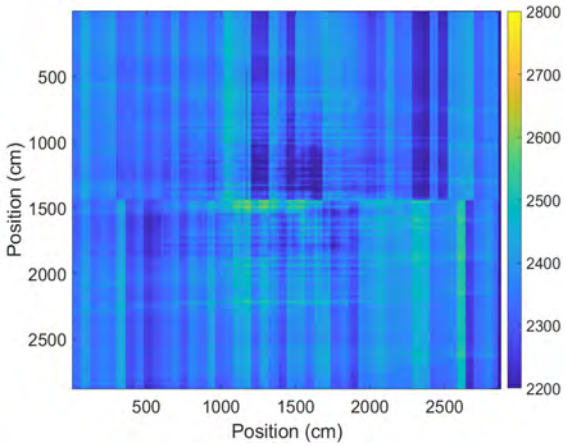

(b) Intensity map representing the difference between the raw and corrected image acquired with D1.

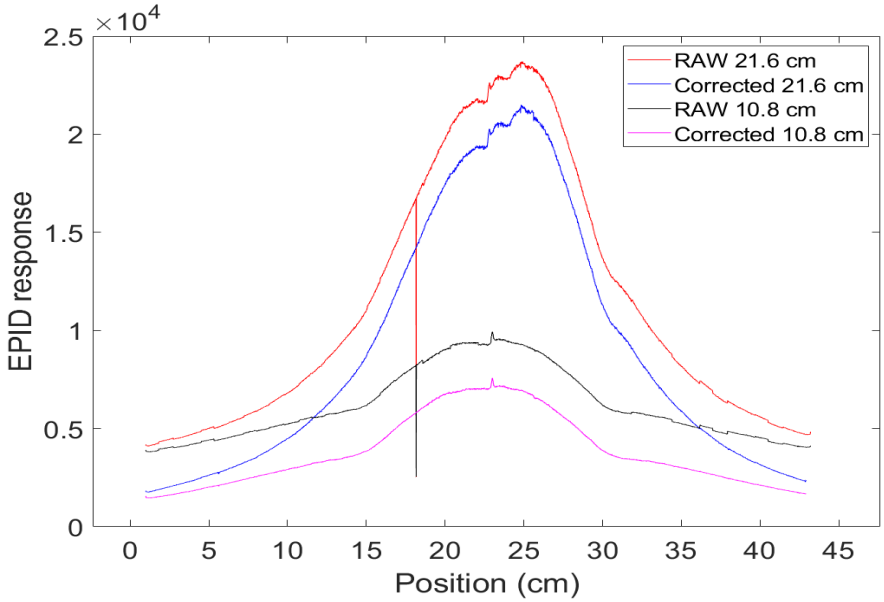

(c) Intensity profile before (RAW) and after (Corrected) the response corrections of D1

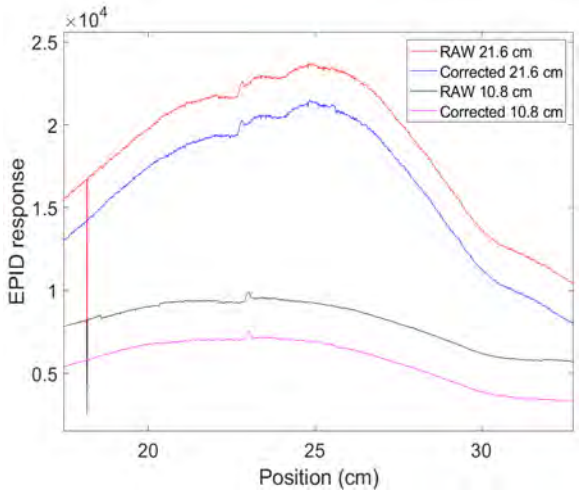

(d) Intensity profile of D1 zoomed in on the peak region

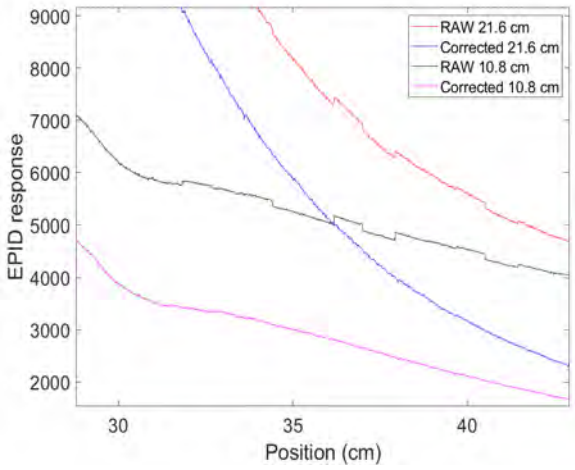

(e) Intensity profile of D1 zoomed in on the boundary region

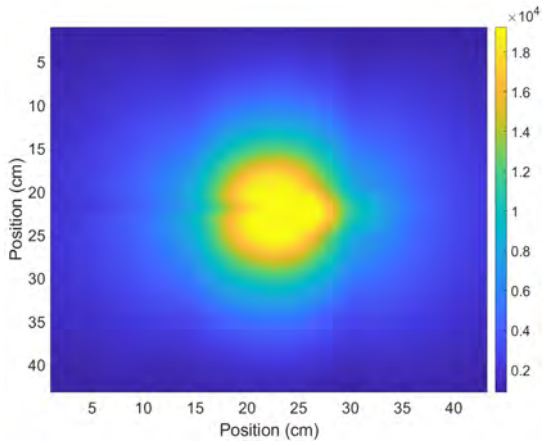

(f) Image after response corrections acquired with D2

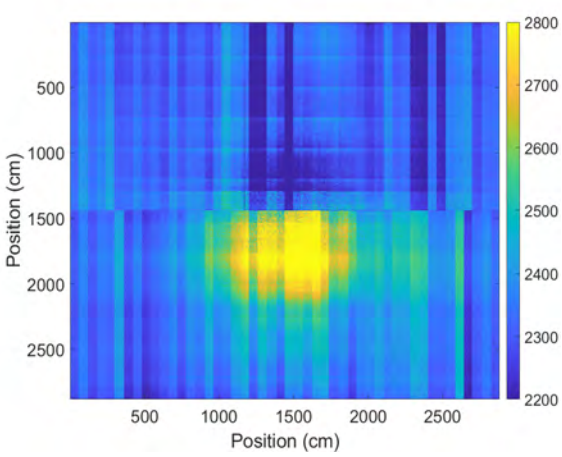

(g) Intensity map representing the difference between the raw and corrected image acquired with D2.

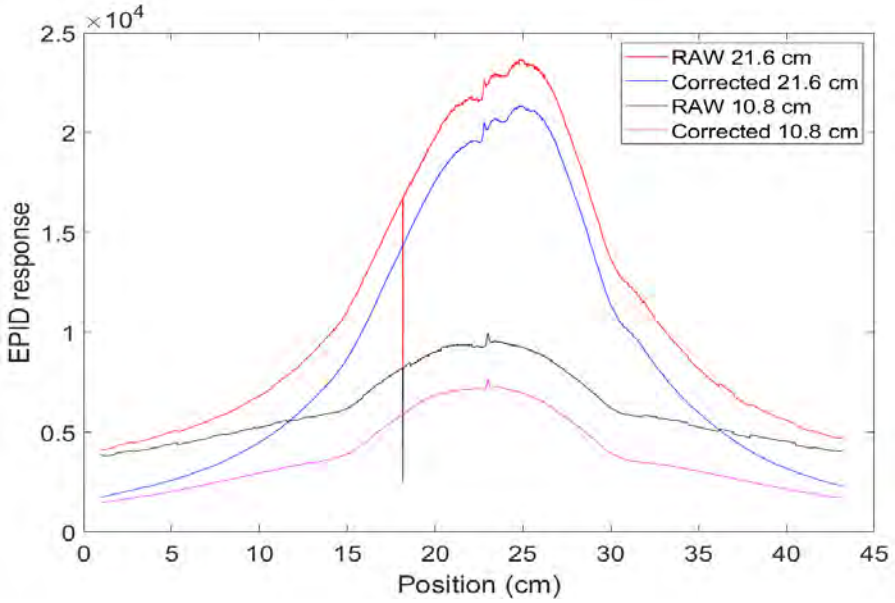

(h) Intensity profile before (RAW) and after (Corrected) the response corrections of D2

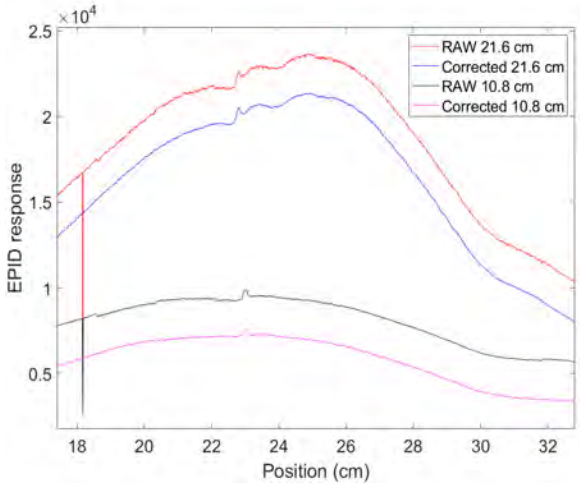

(i) Intensity profile of D2 zoomed in on the peak region

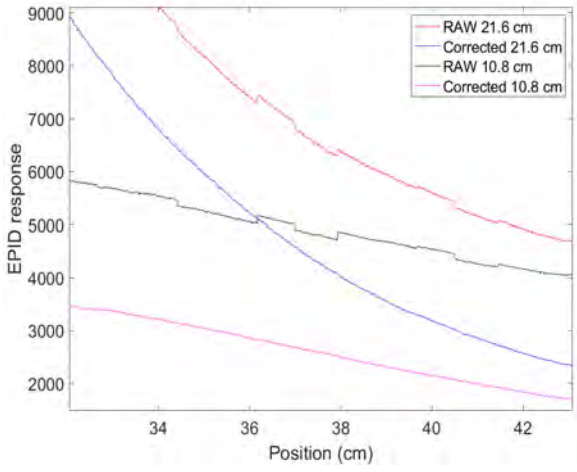

(j) Intensity profile of D2 zoomed in on the boundary region

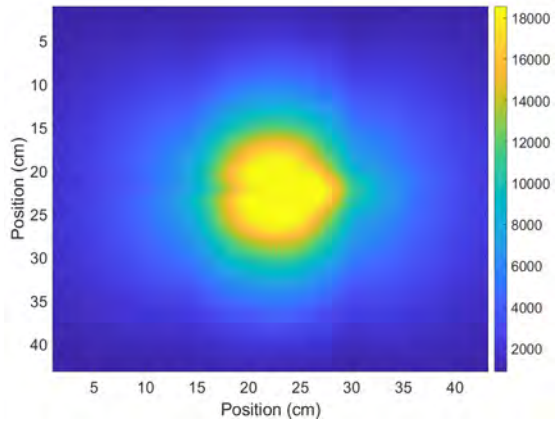

(k) Image after response corrections acquired with D3

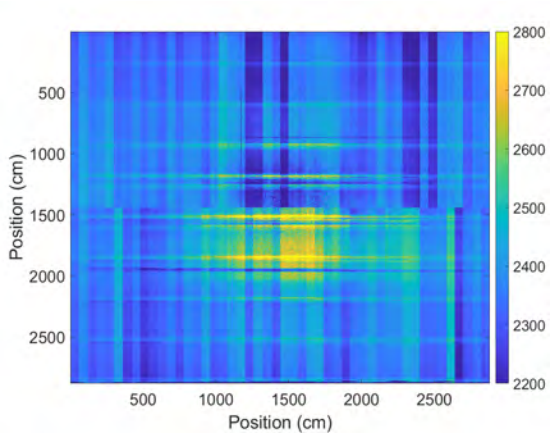

(l) Intensity map representing the difference between the raw and corrected image acquired with D3.

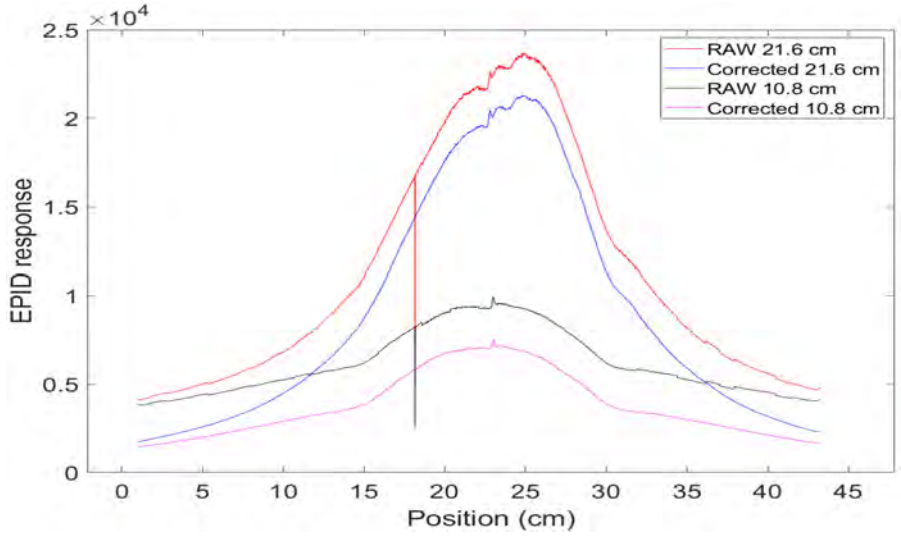

(m) Intensity profile before (RAW) and after (Corrected) the response corrections of D3

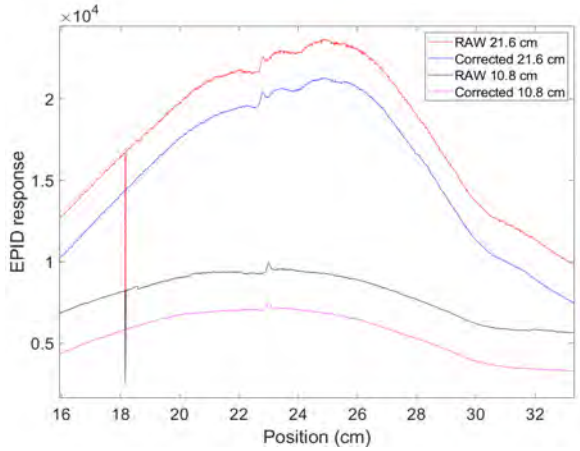

(n) Intensity profile of D3 zoomed in on the peak region

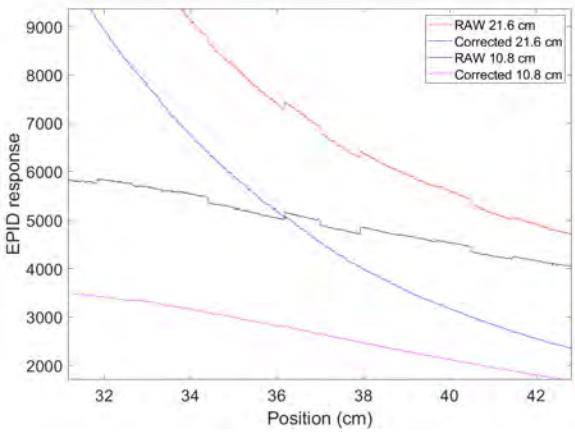

(o) Intensity profile of D3 zoomed in on the boundary region

Figure 6: Evaluation on an independent image (gain mode = 5, binning = 1x1, frame rate = 9 fps) acquired with HDR Ir-192 source. The intensity profiles at panel positions 21.6 cm and 10.8 cm showing the data without correction (RAW) and with the correction of the DF, DL, PSM (Corrected) of each dataset.

panel position 18 cm on the x-axis in the RAW image (Figure 4) and in all intensity plots (Figures 6c, 6h and 6m). After DL correction, the artefact line has been replaced with the neighbouring pixel values and is neither visible in the image nor intensity profile. Hence, it can be confirmed that the noise level improves after the DF and DL correction since Table 3 shows around 20% higher N_{imp} values for each dataset compared to Table 4.

For PSM1 (Figure 5a), the horizontal lines appear at almost all positions on the panel. This is due to the fact that the EPID is not synchronized with the linac. So when the EPID is being read out, the EPID is still receiving a radiation pulse from the linac. This becomes visible during acquisition of the images and appear as horizontal lines in the frames. Since the synchronization problem has not been taken into account during the acquisition of the frames and have not been corrected when deriving PSM1, these lines have effect on the pixel sensitivity of all pixels. Looking at the intensity profiles (Figures 6c and 6d), the noise is not reduced after correction. This can be confirmed according to Table 4, the value of N_{imp} is negative for both panel positions (21.6 cm and 10.8 cm) which indicates that the noise level has even increased when applying the PSM1 correction on the evaluation image. Furthermore, looking at PSM2 and PSM3, there are also several horizontal lines appearing on the panel but are different from PSM1. These lines occur because the EPID has been displaced between each irradiation and when acquiring the PSM, the shift is still visible. However, these lines do not have a negative effect on the evaluation image. Observing the intensity profiles of PSM2 and PSM3 (Figures 6h, 6i, 6m and 6n), the noise level has been reduced for the corrected image at both panel positions. Table 4 also confirms that the noise level improves after correction since the the value of N_{imp} is positive for both positions. Overall, the results are the best for the correction with PSM3, followed by PSM2.

The boundaries of PSM1 and PSM3 contain some dark blue lines. The pixels located in the dark blue line region have not been irradiated with the field. Therefore, another shift of the panel should have taken place to cover these pixels. Since the pixels at the boundaries are not relevant in the evaluation of the calibration method, this was not an issue. Also, when calculating the noise levels of the intensity profiles, the pixel values located at the boundary have been excluded on purpose.

The benefit of this EPID is that the calibration method performs well on images acquired with different settings. This way, the PSM correction can be applied on all kind of images. However, this study has shown some limitations. First, it is not possible to conclude that the calibration method using the MV-source did not perform well since there was not a correction method applied to this dataset. This was due to the fact that only the averaged image has been obtained instead of all individual frames. If the individual frames have been acquired for D1, then the calibration method of D3 could be performed on D1 which could give a better result. Secondly, for D2, the frames are averaged over 1000 frames such that the horizontal lines will not appear in the final averaged image. This method proved to work, however, this is not the optimal method since each pixel contains a certain error. Also, more acquisition time is necessary since many frames need to be acquired. For PSM3, the frames containing the horizontal lines have been excluded to calculate the final averaged image. This method has shown the best results since it guarantees a homogeneous response of the panel and reduces artefacts in the image.

For future research, it is important to look into the synchronization of the EPID with the linac and CBCT. Since the EPID readout should be synced with the beam pulses, the time between the acquisitions needs to be determined. This way, a horizontal line will not be acquired in a frame as the EPID is not readout during a pulse. This can be synchronized by trial and error. A method is to set the frame rate of the detector, acquire the frame and evaluate if the horizontal line is not present in this frame. If the horizontal line is present, the frame rate should be adjusted. By solving the synchronization problem, the calibration method will be more accurate since all frames can be taken into account and it also reduces the acquisition time. However, if the synchronization cannot be determined, the calibration method acquired with D3 can be used since it showed positive results. It is recommended to acquire more frames since the average image discarded at least one third of the 100-120 frames. This is due to the fact that the first and last ten frames contain lower intensity values compared to the median pixel value of all frames per pixel location (ghosting) and about twenty frames have been excluded since the horizontal lines appear in these frames. In addition, since the calibration method acquired with D3 performed well, this method could also be performed on a dataset acquired with the linac to see if a higher energy source could give a better calibration result of the EPID. However, the risk of damaging the electronics of the EPID still exists.

5 Conclusion

In this study, a pixel sensitivity correction of the EPID has been determined to eventually improve images acquired with a HDR brachy source. It can be concluded that the calibration method acquired with D3 performed the best since the noise level in the corrected evaluation image has been reduced with

52.5 to 54.8% with respect to the RAW image. Also, this corrected image has improved since the panel has given a homogeneous response and artefacts are reduced in the image. For future reference, the synchronization of the EPID with the linac and CBCT should be looked into.

References

[1] C. Anderson, P. Fleming, A. Wilkinson, and A. D. Singh, *Principles of Radiation Therapy*. Elsevier Inc., 2007, pp. 40–44.

[2] S. J. Otter, A. J. Stewart, and P. M. Devlin, "Modern Brachytherapy," *Hematology/Oncology Clinics of North America*, vol. 33, no. 6, pp. 1011–1025, 2019.

[3] K. Tanderup, C. Ménard, C. Polgar, J. C. Lindegaard, C. Kirisits, and R. Pötter, "Advancements in brachytherapy," *Advanced Drug Delivery Reviews*, vol. 109, pp. 15–25, 2017.

[4] G. P. Fonseca, M. Podesta, M. Bellezzo, M. R. Van Den Bosch, L. Lutgens, B. G. Vanneste, R. Voncken, E. J. Van Limbergen, B. Reniers, and F. Verhaegen, "Online pretreatment verification of high-dose rate brachytherapy using an imaging panel," *Physics in Medicine and Biology*, vol. 62, no. 13, pp. 5440–5461, 2017.

[5] G. P. Fonseca, J. G. Johansen, R. L. Smith, L. Beaulieu, S. Beddar, G. Kertzscher, F. Verhaegen, and K. Tanderup, "In vivo dosimetry in brachytherapy: Requirements and future directions for research, development, and clinical practice," *Physics and Imaging in Radiation Oncology*, vol. 16, no. April, pp. 1–11, 2020.

[6] G. P. Fonseca, T. Van Wagenberg, R. Voncken, M. Podesta, C. Van Beveren, E. Van Limbergen, L. Lutgens, B. Vanneste, M. Berbee, B. Reniers, and F. Verhaegen, "Brachytherapy treatment verification using gamma radiation from the internal treatment source combined with an imaging panel - A phantom study," *Physics in Medicine and Biology*, vol. 66, no. 10, 2021.

[7] J. W. Wong, "Electronic Portal Imaging Devices (EPID)," *Encyclopedia of Radiation Oncology*, pp. 207–213, 2013. [Online]. Available: `https://link.springer.com/referenceworkentry/10.1007/978-3-540-85516-3_33`.

[8] Varex Imaging Corporation, *XRD 4343N Flat Panel Detector*, 2020.

[9] L. Parent, A. L. Fielding, D. R. Dance, J. Seco, and P. M. Evans, "Amorphous silicon EPID calibration for dosimetric applications: Comparison of a method based on Monte Carlo prediction of response with existing techniques," *Physics in Medicine and Biology*, vol. 52, no. 12, pp. 3351–3368, 2007.

[10] A. Boriano, F. Lucio, E. Calamia, E. Russi, and F. Marchetto, "A new approach for the pixel map sensitivity (PMS) evaluation of an electronic portal imaging device (EPID)," *Journal of Applied Clinical Medical Physics*, vol. 14, no. 6, pp. 234–250, 2013.

[11] G. P. Fonseca, "Dose and motion measurements in brachytherapy (DETERMINE), grant application," pp. 1–24, 2019.

[12] Varex Imaging Corporation, *XRD 4343N — Varex*, 2019. [Online]. Available: `https://www.vareximaging.com/products/flat-panel-detectors/xrd-4343n`.

[13] P. B. Greer, "Correction of pixel sensitivity variation and off-axis response for amorphous silicon EPID dosimetry," *Medical Physics*, vol. 32, no. 12, pp. 3558–3568, 2005.